CHEMISTRY
A European Journal

A Journal of
ChemPubSoc Europe

Accepted Article

Title: Elucidating the Structure-Reactivity Correlations of Phenothiazine based Fluorescent Probes toward ClO□

Authors: Shichao Wang, Boyu Zhang, Wenjing Wang, Gang Feng, Daqiang Yuan, and Xuanjun Zhang

To be cited as: *Chem. Eur. J.* 10.1002/chem.201800356

Link to VoR: http://dx.doi.org/10.1002/chem.201800356

Supported by
ACES

WILEY-VCH

10.1002/chem.201800356

WILEY-VCH

Elucidating the Structure-Reactivity Correlations of Phenothiazine based Fluorescent Probes toward ClO⁻

Shichao Wang,[a] Boyu Zhang,[a] Wenjing Wang,[b] Gang Feng,[a] and Daqiang Yuan, *[b] Xuanjun Zhang*[a]

Abstract: In this work, with the aim to develop effective molecular probes and investigate the structure-reactivity correlation, we designed a short series of phenothiazine based fluorescent probes for detecting ClO^- with differing electron push-pull groups. Sensing experiment results and single crystal X-ray analysis with the aid of TD-DFT calculation revealed that substituting groups with increasing electron-withdrawing ability could increase the dihedral angle of phenothiazine moiety and reduce the gap energy of probes, which led to enhanced reactivity towards ClO^-. Both **PT1** and **PT2** showed two-color switching upon detection of ClO^-. **PT1** with strong electron donating group thiophene showed fluorescence color switch from salmon to blue. **PT2** with medium electron donating/accepting group benzothiazole showed a fluorescence color switch from red to green. However, both **PT1** and **PT2** almost had no response to $ONOO^-$. Through introducing strong electron-withdrawing ketone combined with a cyano group, **PT3** showed a cyan emission upon detection of ClO^- and weak red emission upon detection of $ONOO^-$. HRMS and ^1H NMR results confirmed that **PT1** and **PT2** had the same sensing mode, in which the divalent sulfur of phenothiazine could be oxidized to sulfoxide by ClO^-. When reacted with ClO^-, **PT3** experienced two-step reactions. It was firstly oxidized into sulphone structure by ClO^- and then transformed into sulfoxide phenothiazine aldehyde. When encountered $ONOO^-$, **PT3** changed into aldehyde structure and some non-fluorescence byproducts. Owing to their special selectively and high sensitivity, **PT1** and **PT2** were applied to image the endogenous ClO^- in macrophage cells and zebrafish larvae. This study was expected to provide a useful guideline for probe design for various applications.

Introduction

Reactive oxygen species (ROS) are produced from molecular oxygen in cellular redox activities, which played a variety of roles in biological and pathological processes. [1] Small fluorescent probes are essential molecular tools for detecting the ROS in the biological system as they demonstrated the prominent advantages of high sensitivity and easy accessibility. [2] To date, a great many of new small fluorescent probes for detecting various ROS have been reported. [3] However, due to the aggressive oxidability of ROS, it was challenging to monitor the reactions in sensing process. Hitherto, though the sensing mechanisms of some sole probes were briefly proposed in some reports, there were few literatures presented a relationship between the sensing mechanism and the molecular structures among a series of probes. It brought some confusion that some analogous probes had a great difference in responding speed, sensing mode or fluorescence signal change towards the same ROS. For example, the similar aromatic boronates probes **TCFB1** and **TCFB2** had a different sensitivity to peroxynitrite ($ONOO^-$), **TCFB2** even had a great difference in responding to $ONOO^-$ and hypochlorous acid (HClO) in almost the same buffer.[4] The two-photon fluorescent probe of naphthalimide derivatives with dimethylthiocarbamate group (**NDMTC**) had a fast respond to HOCl, while similar probe **NDMC** with dimethylcarbamate group had no response.[5] The parallel donator-π-acceptor (D-π-A) type phenothiazine-based fluorescent probes displayed chaotic detection for hydroxyl radical (·OH), ClO^- and disparate reacted products. [6] Although significant progress has been made, it was still hard to conclude an adaptive rule to govern the rational design of probes.

In this work, with the aim of exploring sensing rule of probes toward ROS, we designed a short series of phenothiazine based molecular probes for the detection of ClO^-, and try to elucidate the structure-reactivity correlation. Phenothiazine as an easy-functionalized and electron rich donator demonstrated the distinct advantage in the design of molecular probes. [7] ClO^- as a hROS, which had aggressive oxidability bearing complex reaction mode with probes. To adjust the reacting activity of probes, we substituted different pushing-drawing electron groups on the phenothiazine framework bridging by cyanostilbene (**Scheme 1**) to increase the intramolecular charge transfer (ICT). The crystal analysis and theoretical calculation revealed that increased dihedral angle of phenothiazine could enhance the ICT effect and promote reaction activity of probes

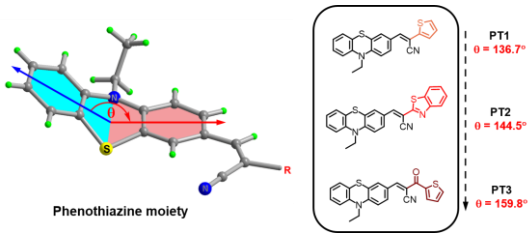

Scheme 1. The structures of target probes **PT1**, **PT2** and **PT3**

[a] S. Wang, Dr. B. Zhang, G. Feng, Prof. Dr. X. Zhang
Faculty of Health Sciences
University of Macau
Taipa, Macau SAR, China
E-mail: xuanjunzhang@umac.mo
[b] Dr. W. Wang, Prof. Dr. D. Yuan
State Key Laboratory of Structural Chemistry, Fujian Institute of Research on the Structure of Matter
Chinese Academy of Sciences
Fuzhou 350002, China
E-mail: ydq@fjirsm.ac.cn

Supporting information for this article is given via a link at the end of the document.

towards ClO^-, thus lead to the different sensing modes for three probes.

Results and Discussion

Photophysical properties, crystal structures and computational studies

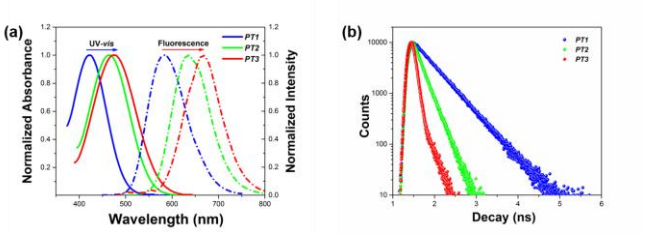

Figure 1. (a) Normalized UV–*vis* absorption and fluorescence spectra of **PT1 ~ PT3** in THF with a concentration of 10^{-5} mol·L^{-1}; (b) Time-resolved fluorescence curves of **PT1 ~ PT3** in THF with a concentration of 10^{-5} mol·L^{-1}.

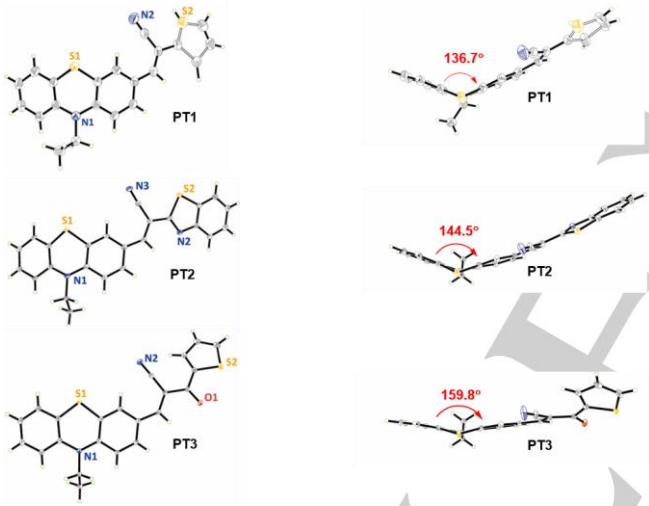

Figure 2. The crystal overlook and lateral views of single molecules **PT1 ~ PT3**, the graphs were obtained by XP software.

Linear absorption spectra of the three molecules in THF was depicted in **Fig. 1** and **Fig S2**. The corresponding photophysical data were summarized in **Table S1**. All three probes displayed dual intense absorption bands in the 310–478 nm range. The high energy absorption bands (310 ~ 340 nm, ε > 10000 mol^{-1}·L·cm^{-1}) were ascribed to π-π* transition of the phenothiazine moiety. [8] The latter low energy absorption bands (422 ~ 478 nm, ε > 10000 mol^{-1} ·L·cm^{-1}) were considered as intramolecular charge transfer (ICT) transition. **PT2** has a longer absorption band than **PT1** due to the stronger electron-withdrawing ability of benzothiazole than thiophene which lead to stronger ICT. **PT3** had the lowest energy absorption band among three molecules, which indicated that the cyano combined with a carbonyl group could strengthen the electron-withdrawing ability and thus further red shift its absorption. The fluorescence emission (**Fig. 1, Fig. S2b**) showed a similar red shift tendency from **PT1** to **PT3**, which also indicated that higher electron-withdrawing groups could increase the ICT in the conjugated system and lower the energy of excited state.

To investigate the relationship between the molecular structures and photophysical properties, single-crystal X-ray diffraction was conducted for all three molecules. The crystals data collection and refinement parameters were listed in **Table S2**. The molecular structures were showed in **Fig. 2** and **Fig. S3**. **PT1** crystallized in *Pbca* system with orthorhombic space group, **PT2** and **PT3** crystallized in *P2(1)/n* system with monoclinic space group. The dihedral angles of phenothiazine moiety in **PT1** to **PT3** were 136.7°, 144.5° and 159.8°, respectively (**Fig. 2**). This result revealed that the stronger electron-withdrawing substituent group could draw the phenothiazine moiety more flat. The rigid flat structure can facilitate the intramolecular charge transfer.[9]

To elucidate the relationships between the structures and optical properties of three molecules, theoretical calculation (TD-DFT) based on their crystal structures for absorption properties were carried out. The spatial plots of selected TD-DFT frontier molecular orbits were shown in **Fig. 3**. The calculated result of linear absorption of three molecules in the gas phase was listed in **Table S3**.

As shown in **Fig. 3**, the HOMOs (H and H - 1) of **PT1** located across the whole framework, and LUMOs (L) mainly located on the cyanostilbene area and thiophene group. **Table S3** showed that the energy absorption peak (422 nm) of **PT1** experimentally measured was consistent with theoretical value (427.84 nm), where was associated with a charge transfer transition from HOMO-1 to LUMO. For **PT2**, likewise, the HOMO-1 located on the whole structure. HOMO mainly located on phenothiazine moiety and ethylene bond. After excitation, the LUMOs mainly located on the cyanostilbene area. It also indicated **PT2** had a charge transfer transition from phenothiazine to cyanostilbene group. The measured absorption peak (465 nm) well agreed

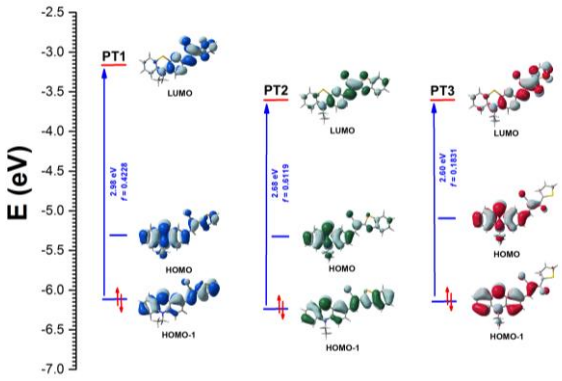

Figure 3. Spatial plots of selected frontier molecular orbits of **PT1 ~ PT3** (TD-DFT/ B3LYP).

with theoretical value (463.10 nm), which was also associated with a charge transfer transition from HOMO-1 to LUMO. The HOMOs of **PT3** located on phenothiazine moiety entirely, and LUMOs located on cyano and carbonyl group, which showed the strongest ICT among three molecules. The excited energy of three molecules shown that **PT3** had the lowest excited energy (2.60 eV) compared with **PT2** (2.68 eV) and **PT3** (2.98 eV). It could be concluded that the strong electron withdrawing group decreased the HOMO or LUMO energy levels, and then decreased the HOMO–LUMO energy gaps. Therefore, it was reasonable that the maximum absorption and emission peaks of **PT3** measured exhibited longer wavelengths than those of **PT1, PT2**. In addition, from **PT1** to **PT3**, there will be an increased activity upon external stimuli because of reduced excited energy.

Photophysical properties of PT1 ~ PT3 for ClO⁻ detection

The reactivity of three probes toward different ROS was assessed including NO, H_2O_2, ·OH, ClO^-, $ONOO^-$, GSH, and TBHP. Various species of ROS (100 μM) were added to the solution of **PT1 ~ PT3** (10 μM) in 0.05 M PBS buffer (pH 7.4, 0.05 M, containing 10% CH_3CN), respectively. The photophysical parameters were summarised in **Table S4**. As shown in **Fig. S4**, upon addition of 10 equivalent ROS species, the color of the **PT1** solution kept stable except for ClO^- changed from light yellow to colorless (inset of **Fig. S4**), accompanied by a blue shift of absorption peak from 423 nm to 378 nm. The fluorescence of **PT1** changed from orange (622 nm) to blue (446 nm) emission under a hand-held UV lamp (**Fig. S4**). **PT1** showed a dramatic increase in ratiometric fluorescence response (I_{446}/I_{622}) of 137 folds towards ClO^- (**Fig. 4(a3)**), while other ROS exhibited a negligible response (< 0.02 folds). These result indicated that **PT1** had a highly specific selectivity for ClO^- over other ROS. Similar events were observed with **PT2** in the presence of various ROS. Upon reacting with 10 equivalent ClO^-, the solution color turned from brown to colorless with the absorption peak shifted from 468 nm to 407 nm (**Fig. S5(a)**). Meanwhile, the fluorescence changed from red (665nm) to green emission (516 nm) (**Fig. S5(b)**). The other ROS had little effect on its absorption and fluorescence except for $ONOO^-$, which induced a slight fluorescence change (inset of **Fig. S5(b)**). But the ratiometric respond (I_{516}/I_{665}) of $ONOO^-$ (2.1 folds) was negligible compared with ClO^- (47.3 folds), which indicated that **PT2** also had an excellent specific selectivity for ClO^- (**Fig. 4(b3)**). Particularly, **PT3** had a response to both ClO^- and $ONOO^-$ with the color change from pink to colorless (inset of **Fig. S6(a)**). Because of strong ICT effect, **PT3** showed a complete quenching fluorescence in a polar medium of PBS

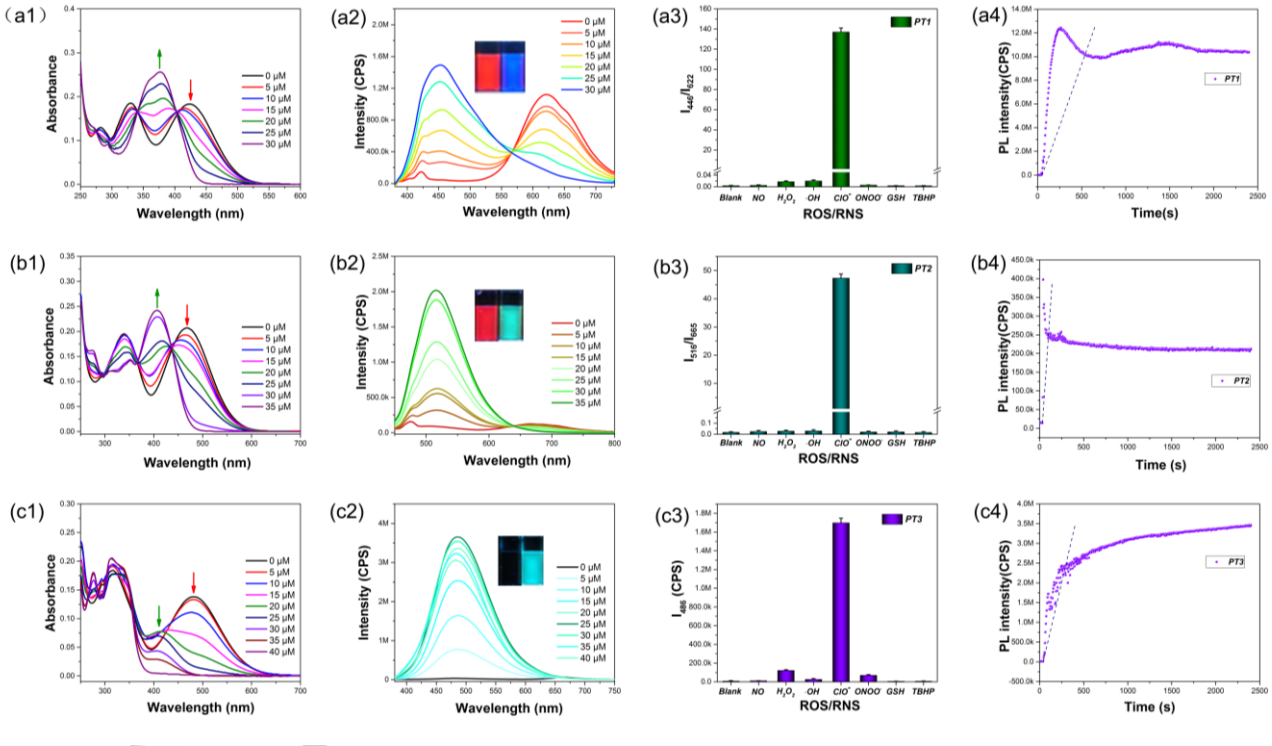

Figure 4. (**a1, b1, c1**) UV-vis absorption spectrum changes of **PT1 ~ PT3** (10 μM) after reaction with different concentrations of ClO^- (0 ~ 35 μM, 0 ~ 35 μM, 0 ~ 40 μM) in 0.05 M PBS:CH_3CN (v:v=9:1) of pH 7.4 for 30 minutes. (**a2, b2, c2**) Fluorescence spectrum changes of **PT1 ~ PT3** responding to absorption in the same condition. (**a3, b3, c3**) Relative fluorescence intensities of the **PT1 ~ PT3** (10 μM) treated with various ROS and RNS in 0.05 M PBS:CH_3CN (v:v=9:1) of pH 7.4 for 90 min. NO: 100 μM; H_2O_2: 100 μM; ·OH: 100 μM + 100 μM ferrous ammonium sulfate; OCl^-: 100 μM NaClO; $ONOO^-$: 100 μM NaONOO; GSH: 100 μM; TBHP: 100 μM. (**a4, b4, c4**) Time dependent fluorescence intensity changes of **PT1 ~ PT3** (10 μM) in the presence of 10 equiv. ClO^- in 0.05 M PBS:CH_3CN (v:v=9:1) of pH 7.4 for 40 min. The fluorescence intensity point was recorded every 5 seconds, 481 points in total. ($\lambda_{ex\text{-}PT1}$ = 380 nm, $\lambda_{ex\text{-}PT1}$ = 446 nm; $\lambda_{ex\text{-}PT2}$ = 410 nm, $\lambda_{ex\text{-}PT2}$ = 516 nm; $\lambda_{ex\text{-}PT3}$ = 315 nm, $\lambda_{ex\text{-}PT3}$ = 486 nm)

buffer. Upon detection of ClO^-, high-intensity cyano emission (486 nm) was observed. But the probe treated with the same equivalent $ONOO^-$ had a very weak orange emission fluorescence (**Fig. S6(b)**). This implied that **PT3** was possibly decomposed into some non-fluorescence byproducts by $ONOO^-$. The above results indicated that **PT3** had a higher reactive activity towards $ONOO^-$ among three probes.

To investigate the sensing mechanism, the titration experiments of the three probes (10 μM) were conducted in PBS buffer (pH 7.4, 0.05 M, containing 10% CH_3CN). As shown in **Fig. 4(a1)**, upon addition of ClO^- from 0 to 30 μM, **PT1** showed a decreasing absorption peak at 423 nm and an emerging peak at 378 nm increased. Meanwhile, the fluorescence peak intensity at 622 nm decreased and 446 nm increased (**Fig. 4(a2)**). Based on the fluorescence titration (**Fig. S7(a)**), the ratio of fluorescence intensity at 446 nm was linearly related to the ClO^- concentration between 0 and 30 μM, with a low detection limit of 0.515 μM defined as the concentration corresponding to triple standard deviations of the background signal ($3\sigma/k$). **PT2** had a similar performance with **PT1** in the presence of ClO^- from 0 to 35 μM, the original absorption peak at 468 nm decreased and an emerging peak at 407 nm increased gradually. The fluorescence emission at 665 nm decreased and 516 nm increased with the increase of ClO^-. The detection limit was calculated as 0.275 μM within linearly related to the ClO^- concentration between 0 and 35 μM. **PT3** displayed a distinctive absorption spectrum, which showed a decreased peak at 482 nm firstly upon addition of ClO^-. When the amount of ClO^- reached around 20 μM, a new absorption peak at 410 nm emerged and faded to disappear with the continued increase of ClO^- about 40 μM (**Fig. 4(c1)**). The fluorescence intensity at 486 nm increased firstly until 25 μM ClO^-, and then decreased (**Fig. 4(c2)**). Through fitting the linear relation of ClO^- concentration between 0 and 20 μM, the detection limit of **PT3** was obtained as the lowest value of 0.139 μM. Thus, three probes all had a very high sensitivity for ClO^- and well to detect ClO^- *in vitro* by ratiometric means at low concentrations. The detect limits also indicated an increased reactive sensitivity to ClO^- from **PT1** to **PT3**, which was accordance with front speculation of TD-DFT theoretical calculation. Besides, **PT3** also had a response to $ONOO^-$ without a regular change of absorption and fluorescence (**Fig. S8**).

We further tested the time-dependent fluorescence intensity changes of **PT1 ~ PT3** (10 μM) in the presence of 10 equivalent ClO^- in PBS buffer (pH 7.4, 0.05 M, containing 10% CH_3CN). As shown in **Fig. 4 (a4, b4, c4)**, **PT1**, **PT2**, and **PT3** all had a fast response to ClO^- in PBS buffer about 538 s, 100 s, and 304 s, respectively. **PT2** had a faster response to ClO^- than **PT1**, which was likely to that the ClO^- oxidized phenothiazine of **PT2** to sulfoxide more easily. **PT3** had a relatively long response time due to the possible coexistence of multiple steps oxidation reactions towards ClO^- according to its absorption and fluorescence spectrums change. In addition, we proceeded to examine the effect of pH on fluorescence of three probes. Little influence on **PT1** and **PT2** within a wide pH range (4-10), indicated that no disturbance from the variation of pH. But for **PT3**, there was an obvious absorption and fluorescence decrease in pH 9 ~ 10 (inset of **Fig. S9**). Considering the sensitivity and fluorescence intensity before and after reaction with ClO^-, both **PT1** and **PT2** were expected to be useful tools for biological and pathological investigations.

The proposed sensing mechanism of PT1–PT3 towards ROS

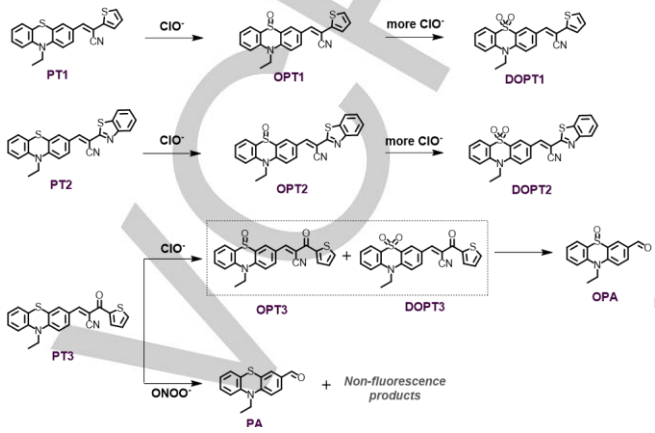

Scheme 2. Proposed sensing mode of **PT1 ~ PT3.**

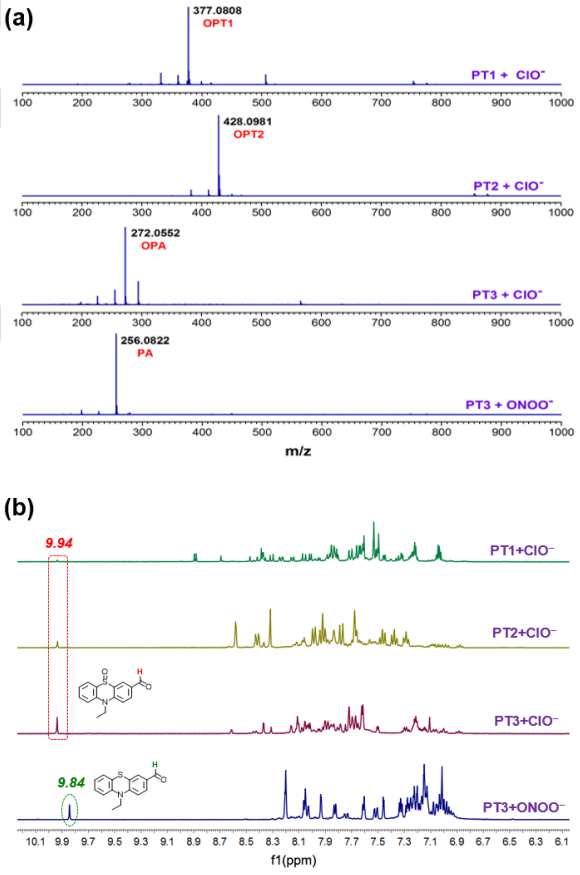

Figure 5. (a) The HR-MS spectrum of product of **PT1 ~ PT3** (10 μM) after reacted with 10 equiv. ClO^- and $ONOO^-$ for 10 minutes, respectively. (b) The ^{1}H-NMR spectrum of **PT1**, **PT2** treated with 10 equiv. ClO^-, **PT3** treated with10 equiv. ClO^- and $ONOO^-$ for 10 minutes.

Based on the experimental results, the sensing mechanisms were proposed, which were demonstrated in Scheme 2. **PT1–PT3** all had two activated sites sulfur atom of phenothiazine and double bond which had higher electron density and can be effectively oxidized or cut off by ClO^-. Besides, we abandoned activated sites sulfur atoms of thiophene (**PT1, PT3**) and benzothiazole (**PT2**) because they were hardly oxidized for their electron-deficiency compared with the sulfur atom on the phenothiazine moiety. [10] Here, to clear the sensing mode of probes towards ClO^- and $ONOO^-$, the reactions products of **PT1 ~ PT3** were determined by HR-MS (positive mode), ^{1}H-NMR data and TD-DFT theoretical calculation (**Fig. 5, Fig. S10 ~ Fig. S13, Fig. 6**).

Fig. 5(a) displayed the HR-MS spectrum of probes (10 μM) after reacting with ClO^- (100 μM) and $ONOO^-$ (100 μM, just for **PT3**) for 30 minutes. The HPLC HR-MS analysis showed a main mass peak at 377. 0808 for **PT1** after treating with ClO^-. This peak was assigned as sulfoxide structure (**OPT1**). **PT2** also turned into sulfoxide structure (**OPT2**) responding to main mass peak at 428.0981 after treating with 10 equivalent ClO^-. For **PT3**, in the presence of 10 equivalent ClO^- and $ONOO^-$, the main mass peak 272.0552 and 256.0822 were generated, respectively. They were taken as sulfoxide aldehyde (**OPA**) and aldehyde (**PA**) structures. To detail the reaction process of probes towards ClO^-, the HPLC chromatogram (mobile phase CH_3CN: water = 1: 1, v/v; 0.2 ml·min^{-1}) and HR-MS spectrums of probes reacted with different equivalent ClO^- for 30 minutes were depicted. The **Fig. S10** showed the HPLC chromatogram of different equivalents (25 μM, 50 μM, 100 μM, 200 μM, 300 μM) ClO^- reacted with **PT1** (10 μM) in pH 7.4 PBS buffer. In the presence of 25 μM of ClO^- or below, **PT1** partially turned into **OPT1**. Under 100 μM of ClO^- amount, **PT1** mainly turned into **OPT1** corresponding to mass peak at 377.0808. The generation of **OPT1** was also supported by the blue fluorescence. When the concentration of ClO^- increased to 200 μM, the sulphone structure product (**DOPT1**) was generated corresponding to mass at peak 393.0833. At the same time, the mass peak of **OPT1** was observed and **PT1** disappeared completely. It was interesting to note that when the concentration of ClO^- was further increased to 300 μM, **OPT1** disappeared and it was transferred into a new product **DOPT1**. It indicated that **PT1** had a two-step oxidation process upon the extra amount of ClO^-. In the first oxidation step, the ClO^- (100 ~ 200 μM) was in the range of physiological concentration (5 ~ 200 μM) of hypochlorite. [11] **PT2** had a similar two-step oxidation process with **PT1** upon the increase of ClO^- amount responding main mass peaks of 427.0813 (**OPT2**) and 444.0941 (**DOPT2**) (**Fig. S11**). The green fluorescence mainly came from **OPT2**. For **PT3**, treated with different equivalents ClO^- (10 μM, 20 μM, 30 μM, 50 μM, 100 μM) in pH 7.4 PBS buffer, showed two retention time peaks in five equivalents ClO^- reaction solution simultaneously (**Fig. S12**). From 10 μM to 30 μM, the peak of around 2.11 second retention time decreased and the peak of 2.44 second retention time kept stable, these two retention peaks corresponded to the main mass peak at 421.0763 which was assigned as **DOPT3**. The peak of around 1.03 second increased with the increase of ClO^- amount, which was corresponded to the main mass peak at 272.0752 that was identified to **OPA**. It indicated that **DOPT3** and **OPA** coexisted in low and high ClO^- concentrations (10 ~ 100 μM). Similar to **PT1** and **PT2**, **PT3** also experienced the first oxidation process and turned into **OPT3** in the presence of ClO^-. While **OPT3** possessed a very short lifetime and then transformed into **OPA** quickly. The fluorescence signals of probe **PT3** upon detection of ClO^- was primarily generated by both **OPA** and **DOPT3**. **Fig. S13** showed the HPLC chromatogram of four equivalents (10 μM, 20 μM, 50 μM, 100 μM) $ONOO^-$ after reacting with **PT3** for 30 minutes. A peak around 2.52 second retention time existed in all chromatogram, which was corresponded to main mass peak at 256.0822 that hint at aldehyde structure (**PA**). But the unidentified peak and weak orange fluorescence signal also indicated that there was a large amount of non-fluorescence products were produced. The ^{1}H NMR spectrum in deuterated acetone (**Fig. 5b**), the samples of **PT1** and **PT2** after reacted with 10 equivalent ClO^- showed no obvious chemical shift signal at 9.94 ppm, which was assigned as proton peak of aldehyde on sulfoxide phenothiazine. [12] The product of **PT3** after reacting with ClO^- showed a distinct peak at 9.94 ppm indicative of the aldehyde group in sulfoxide phenothiazine product, which agreed with HRMS spectrum. The 9.84 ppm peak in NMR spectrum of **PT3** after treating with $ONOO^-$, combined with HRMS, confirmed the formation of phenothiazine aldehyde. These results revealed that **PT1 ~ PT3** had an increased reactive activity towards ClO^- across the whole oxidation process regularly, which was predicted by crystal analysis and theoretical calculation.

Subsequently, the theoretical calculation of reacted products of probes towards ROS was demonstrated base on optimized structures (**Table S3**, **Fig. 6, Fig. S14**). As shown in **Fig. S14**, the sulfoxide and sulphone phenothiazine products (**OPT1**, **OPT2**, **OPT3**, **DOPT3**, **OPA**) possessed a rich electron density around oxygen atom in ground states and acceptor groups in excited states via ICT. The result of the calculation (**Table S3)**

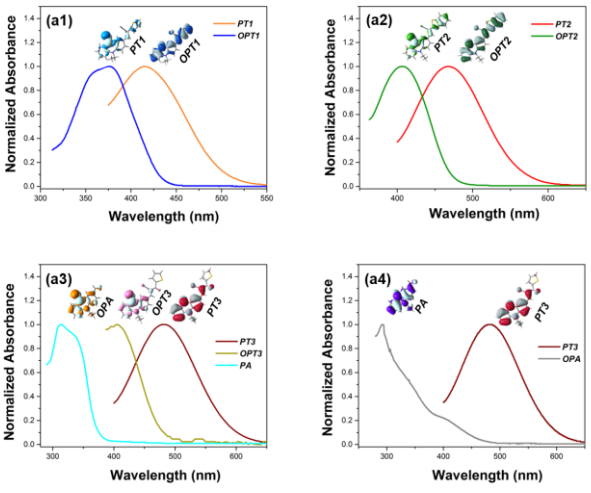

Figure. 6.The normalized absorption spectrum of **PT1**(a1), **PT2**(a2), **PT3**(a3) before and after treating with ClO^-; (a4) **PT3** treating with $ONOO^-$. The inset graphs were the frontier molecular orbits of reactants.

had a good agreement with experimental detection absorption after treating with ClO^- and $ONOO^-$ in **Fig. 6.** The experiment companied with TD-DFT calculation verified the correctness of the sensing mechanism synergistically.

Imaging

Imaging of intracellular ClO^-

Murine RAW264.7 macrophages were used as a ClO^- detection model because it was known to generate ROS and RNS in the immune system. [13] To evaluate the specific nature of **PT1** and **PT2** for detecting the endogenous ClO^-, RAW264.7 cells were taken for imaging by a confocal fluorescence microscope. Lipopolysaccharides (LPS) and phorbol myristate acetate (PMA) were used as the inducer to prompt the cells to generate the ROS. Before imaging, the cytotoxic behaviour of **PT1-2** was examined using the MTT assay with RAW264.7 cells in dose mode. The cells were separately treated with increasing concentration of **PT1, PT2** (5, 10, 20, 40, 60, 80, 100, 120 μM) for 24 h. As shown in **Fig. S15**, there was no obvious cytotoxicity was identified in Raw264.7 cells. The fluorescence imaging of **PT1** and **PT2** for detecting ClO^- in living macrophages Raw264.7cells were demonstrated in **Fig.7**. **Fig. (7(a1), (d1))** displayed a strong red fluorescence emission channel for **PT1** and **PT2** without any LPS and PMA stimulant in 30 minutes. With the addition of 2 $\mu g \cdot mL^{-1}$ LPS and PWA in 1 hour, the Raw264.7 pretreated with 5 μM **PT1** displayed a red fluorescence and blue fluorescence in two channels (**Fig.7(b1, b2)**). For **PT2**, the cells displayed a red fluorescence and weak green fluorescence emission in both channels (**Fig.7(e1, e2)**). The result implied that the generation of endogenous ClO^- was induced by stimulant in Raw264.7 cells. Upon addition of LPS and PWA to 5 $\mu g \cdot mL^{-1}$, the cells treated with **PT1** displayed a very weak red fluorescence and strong blue fluorescence within 1 hour (**Fig.7(c1, c2)**). The cells treated with **PT2** almost displayed only green fluorescence in the green channel (**Fig.7(f1, f2)**). This response should be attributed to the increased concentration of intracellular ClO^- that was stimulated by more LPS and PMA. It confirmed that the **PT1** and **PT2** were capable to detect endogenous ClO^- by two channels in living cells.

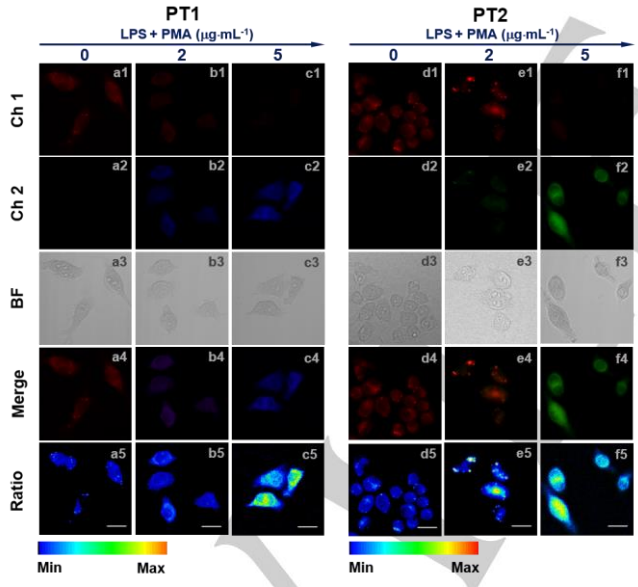

Figure. 7. Confocal fluorescence images for detection of ClO^- production in Raw264.7 cells. (a, d) The cell incubated only with 5 μM **PT1**, **PT2** for 30 minutes, respectively. (b, e) The cells treated with stimulants LPS (2 $\mu g \cdot mL^{-1}$) and PMA (2 $\mu g \cdot mL^{-1}$) for 4 hours in the presence of 5 μM **PT1**, **PT2**, respectively. (c, f) The cells treated with stimulants LPS (5 $\mu g \cdot mL^{-1}$) and PMA (5 $\mu g \cdot mL^{-1}$) for 4 hours in the presence of 5 μM **PT1**, **PT2**, respectively. (a5 ~ f5) The ratio images were generated from **Ch2** and **Ch1**. All images were merged by two channels. The scale bar represented 20 μm.

Imaging of endogenous ClO^- in zebrafish larvae

Zebrafish has been proved to be a valuable vertebrate model due to their prominent advantages such as the similarity in physiology to humans, external fertilization and optical transparency of its embryo and larva.[14] To exhibit the practical application in detecting hypochlorite in intravital imaging, we employed the zebrafish larvae as the animal model. Before we applied the probes in zebrafish larvae imaging, the toxicity of **PT1** and **PT2** were firstly accessed for in vivo tests according to the literature method. [15] Three groups of zebrafish larvae (4-day, 50 zebrafish per group) were fed with different amounts of **PT1, PT2** solutions (10 μM, 20 μM, 30 μM) and were monitored the survival rate for 7 days. It showed that more than 80% survival rate even in the highest concentration, which confirmed that **PT1**

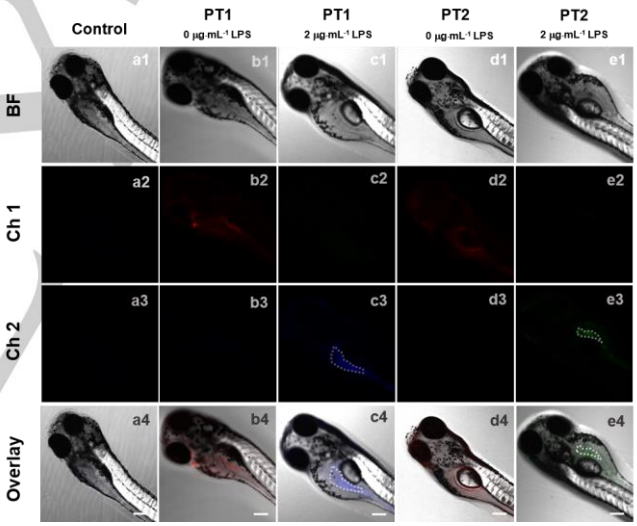

Figure 8. Fluorescence images of **PT1** and **PT2** to detect ClO^- generation by LPS cooperated with PMA induced liver injury in zebrafish larvae. The control group (a1 ~ a4); The zebrafish pretreated with 0 $\mu g \cdot mL^{-1}$ LPS (b1 ~ b4, d1 ~ d4) and 2 $\mu g \cdot mL^{-1}$ LPS (c1 ~ c4, e1 ~ e4) for 6 hours and then incubated with 10 μM **PT1**, **PT2** for 2 hours, respectively. The excitation filter in the range of 405 ~ 488 nm, and the emission filter is 420 ~ 750 nm. Every group was repeated three times. The scale bars represent 200 μm.

and **PT2** were suitable for zebrafish larvae imaging (**Fig. S16**). LPS as an identified inflammatory mediator will lead to acute liver injury along with HClO generation in the process of myeloperoxidase enzyme-mediated peroxidation of chloride ions.[16] The four-day-old zebrafish larvae were incubated with LPS (2 μg·mL^{-1}) for 6 hours, after that, 10 μM **PT1** and **PT2** were fed to larvae for 2 hours, respectively. As shown in **Fig. 8a**, in the control group, there was no any fluorescence signal in the whole body of zebrafish. For larvae which were fed with **PT1** and **PT2** severally, but not pretreated with LPS, displayed the red fluorescence signals around the abdomen area. In contrast, the larvae pretreated with LPS and **PT1** was observed the blue fluorescence signal around the liver and digestive system (white point outline). Likely, the green fluorescence signal was detected around the liver and digestive system of larvae pretreated with LPS and **PT2.** It indicated that fluorescence transformation of probes in zebrafish larvae was triggered by endogenous ClO^-. Probe **PT1** and **PT2** were organism-permeable and sensitive enough to detect the endogenous ClO^- in zebrafish larvae. The result suggested that the two probes had a desirable application for detecting endogenous ClO^- *in vivo* by fluorescence imaging.

Conclusions

Through design and synthesis of a short series of phenothiazine based fluorescent probes **PT1 ~ PT3** composed of different electron donor and acceptor, we investigated the response to ClO^- and structure-reactivity correlation. The probes with the strong push-pull structure could increase the dihedral angle of phenothiazine framework and ICT effect, meanwhile, increased the reactive activity towards ClO^- and $ONOO^-$. The detailed HRMS and ^{1}H NMR spectrum revealed that **PT1** and **PT2** had a rapidly specific absorption and fluorescence response towards ClO^- by oxidation of sulfur to sulfoxide in phenothiazine moiety. With the more ClO^- addition, **PT1** and **PT2** could be further oxidized to sulphone structures. **PT3** went through a complete oxidation process of sulfur to sulphone structures accompanied with sulfoxide phenothiazine aldehyde. **PT3** also had a fast response to $ONOO^-$ by changing into aldehyde structure and some non-fluorescence byproducts. However, **PT1** and **PT2** were inert to $ONOO^-$. Besides, owing to the excellent selectivity and sensitivity, **PT1** and **PT2** were successfully applied to image endogenous ClO^- in macrophage cells and zebrafish larvae. In a word, the detailed study of sensing mechanism and structure-reactivity correlation in this work will give a guideline for further probe design

Experimental Section

Synthesis

The characterizations for all compounds were displayed in supporting materials.

Instruments

Melting point determination was performed on the Buchi B-545 melting point apparatus. FI-IR spectrum was obtained on the SHIMADZU IRAffinity-1S spectrophotometer. The ^{1}H NMR (400 MHz) and ^{13}C NMR (100 MHz) spectra recorded on at 25°C using Bruker AV 400 MHz spectrometers were reported as parts per million (ppm) from tetramethylsilane as the internal standard. High-resolution mass spectra (HRMS) were determined by the electro-spray ionization (ESI) technique and high performances liquid chromatography (HPLC) method which was recorded on the Waters Xevo G2-XS Q-Tof matrix-assisted time of flight mass spectrometer. UV-vis absorption spectra were recorded on a SHIMADZU UV-1800 spectrophotometer. Steady-state fluorescence spectra and time-dependent were performed on HORIBA Fluorolog-3 modular spectrofluorometer with a Xe lamp as an excitation source. Absolute measurement of the fluorescence quantum yield (Φ) of solutions determined by integrating sphere on HORIBA Fluorolog-3 modular spectrofluorometer. Time-resolved fluorescence measurements were also performed on HORIBA Fluorolog-3 platform. The decays were analyzed by "least-squares" and iterative reconvolution method. The quality of the exponential fit was evaluated by the goodness of fit ($\chi 2$).

Measurements

The stock solution of probes **PT1 ~ PT3** (1 mM) were prepared in acetonitrile. The test probes solution (10 μM) were prepared by dilution of stock solution in 0.05 M PBS buffer (pH = 7.4, contain 10% CH_3CN). All aqueous solutions were prepared in ultrapure water with a resistivity of 18.25 MΩ•cm (purified by the Milli-Q system supplied by Millipore, U.S.A). Various ROS and RNS were prepared according to the previous literature.[17] Nitric oxide (NO) stock solution was prepared by purging PBS (0.05 M, pH 7.4) with N_2 gas for 30 minutes and then added NOC-5 at 25 °C. ClO^- was prepared by dilution of commercial sodium hypochlorite solution (available chlorine 10 ~ 15%) in deionized water and the concentration of ClO^- stock solution was determined by measuring the absorbance at 209 nm. H_2O_2 was prepared by dilution of the commercial H_2O_2 solution, the concentration of the stock solution was determined by measuring the absorbance at 240 nm. TBHP were obtained from commercial 70% (w/w) water stock solution. ·OH (hydroxyl radical) was freshly generated by the Fenton reaction from ferrous ammonium sulfate and hydrogen peroxide. $ONOO^-$ was prepared using 3-morpholinosydnonimine hydrochloride, followed concentration determination by UV analysis with the extinction coefficient at 302 nm, the solution was stored at -20 °C for use. Glutathione (GSH) was prepared by dissolving the solid reduced- glutathione in ultrapure water. All test solutions were waited for 40 minutes for measurement after treating with ROS and RNS.

The detection limit ($3\sigma/k$) was obtained based on linear fitting between the fluorescence intensity at 446 nm for **PT1**, 516 nm for **PT2**, 486 nm for **PT3**, and the concentration of ClO^-. σ was the standard deviation of the blank measurements (n = 11), k was the slope of the fluorescence intensity *versus* ClO^- concentration.

Crystallography Determinations

The X-ray diffraction data of three chromophores were collected on a Bruker Smart 1000 CCD area detector diffractometer using graphite monochromated Mo-K_α radiation (λ = 0.71069 Å) at 298(2) K. Empirical absorption corrections were applied to the data. The structures were solved by direct methods and refined by full-matrix least-squares methods on F^2. All the nonhydrogen atoms were located in the trial structure and then refined anisotropically with SHELXTL using the full matrix least-squares procedure. The hydrogen atom positions were geometrically idealized and generated in idealized positions and fixed displacement parameters. Cambridge Crystallographic Data Centre

(CCDC) as supplementary publication numbers CCDC **PT1**-1550369, **PT2**-1540561, **PT3**-1540562.

Computational Studies

The time-dependent density functional theory (TD-DFT/B3LYP) calculations of **PT1~3** were performed on the crystal structures in the gas phase. All calculations were performed with the G03 software. [18] The TD-DFT calculation of the lowest 25 singlet-singlet excitation energies was calculated with a basis set composed of 6-31G (d, p) for C, N, H, O, S atoms. The lowest 25-spin allowed singlet-singlet transitions, up to the energy of about 5 eV, were taken into account for the calculation of the absorption spectra.

MTT Assay

Raw 264.7 macrophage cells were obtained from FHS, University of Macau. In vitro cytotoxicity of **PT1**, **PT2** to Raw264.7 cells was tested by MTT assay. Raw264.7 cells were cultured in 96 wells microplates with Dulbecco's modified Eagle's medium (DMEM) containing 10% fetal bovine serum and maintained at 37 °C in a humidified atmosphere of 95% air and 5% CO_2 for 24 h. The medium was next replaced by fresh medium containing various concentrations of **PT1, PT2** (5, 10, 20, 40, 60, 80, 100, 120 μM) and further cultured another 24 h, respectively. Each concentration was tested in six replicates. Cells were rinsed twice with phosphate buffer saline and incubated with 0.5 mg/mL MTT reagent for 4 hours at 37°C. 100 μL of DMSO was then added to dissolve formazan. The absorbance at 570 nm was measured in a microplate reader. Cell viability (%) was calculated by the following equation: Cell viability = (mean Abs. of treated wells/mean Abs. of control wells) ×100%.

Cell imaging

Raw264.7 macrophage cells were seeded in 25-Petri dishes at an appropriate density about 1×10^3 cells per dish and allowed to adhere for 36 hours. In the control group, the cells were incubated with **PT1**, **PT2** at concentrations 5 μM and maintained at 37 °C in an atmosphere of 95% and 5% CO_2 air for incubation times ranging for 30 minutes. Then the medium was removed and washed the cells with PBS three times (1 mL × 3) to clear dyes attached to the surface of the cells. Meanwhile, in the experimental group, after the macrophage cells have been incubated with 2 $\mu g \cdot mL^{-1}$ LPS and 2 $\mu g \cdot mL^{-1}$ PMA for 4 hours, the cells were further incubated with probes (5 μM) for another 2 hours at 37 °C in an atmosphere of 95% and 5% CO_2 air. The culture was removed and washed with PBS three times (1 mL × 3) before observation. The cells were imaged using Carl Zeiss Confocal LSM710 microscopy with oil immersion lenses. (**PT1**: λ_{ex}: 405 nm and 458 nm, collected λ_{em}: 400 ~ 500 nm and 600 ~ 700 nm; **PT2**: λ_{ex}: 405 nm and 458 nm, collected λ_{em}: 450~ 600 nm and 650 ~ 750 nm).

Fluorescence imaging in zebrafish larvae model

All larval zebrafish were provided by the animal facility of University of Macau. All animal experiments were performed in full compliance with international ethical guidelines and approved by the institutional committee. We have taken great effort to reduce the number of animal in this study and reduced animals suffering from pain and discomfort. All the larval zebrafish were anesthetized using MS222 at level III (Deep Anaesthetized) before microscopy imaging. In the control group, healthy zebrafish larvae (4-day post-fertilization and hatched) were transferred to Petri dishes with 200 μL E3 media (15 mM NaCl, 0.5 mM KCl,1 mM $MgSO_4$, 1 mM $CaCl_2$, 0.15 mM KH_2PO_4, 0.05 mM Na_2HPO_4 and 0.7 mM $NaHCO_3$; pH 7.5) at room temperature for 6 hours. The zebrafish larvae were anesthetized for the subsequent image. To detect the endogenous ClO^-, in the experimental group, zebrafish larvae were transferred to Petri dishes with 200 μL E3 media containing LPS (0 $\mu g \cdot mL^{-1}$, 2 $\mu g \cdot mL^{-1}$) for 6 hours. Then, the media solution was removed and washed the fish three times with 200 μL E3 media to remove remaining LPS. The zebrafish larvae were incubated with E3 media containing 10 μM **PT1** probe and **PT2** probe for another 2 hours at room temperature, respectively. After that, the fish were washed for three times with 200 μL E3 media to remove the residual probes and anesthetized for subsequent fluorescence image. The fluorescence image for zebrafish larvae was carried out on Carl Zeiss Confocal LSM710 microscopy with magnification 5× lenses.

Acknowledgements

This work was supported by the Macao Science and Technology Development Fund under Grant No. 052/2015/A2 and 082/2016/A2; the Multi-Year Research Grant of University of Macau under grant No. MYRG2016-00058-FHS and MYRG2017-00066-FHS.

Keywords: phenothiazine • fluorescence probe • hypochlorous acid • imaging [3g]

[1] aT. Finkel, N. J. Holbrook, *Nature* **2000**, *408*, 239-247; bB. C. Dickinson, C. J. Chang, *Nat Chem Biol* **2011**, *7*, 504-511; cC. Nathan, *J. Clin. Invest.* **2003**, *111*, 769-778.

[2] aX. Li, X. Gao, W. Shi, H. Ma, *Chem Rev* **2014**, *114*, 590-659; bM. Kaur, D. H. Choi, *Chem. Soc. Rev.* **2015**, *44*, 58-77; cY. Tang, D. Lee, J. Wang, G. Li, J. Yu, W. Lin, J. Yoon, *Chem. Soc. Rev.* **2015**, *44*, 5003-5015; dX. Chen, F. Wang, J. Y. Hyun, T. Wei, J. Qiang, X. Ren, I. Shin, J. Yoon, *Chem. Soc. Rev.* **2016**, *45*, 2976-3016; eD. Wu, L. Chen, N. Kwon, J. Yoon, *Chem* **2016**, *1*, 674-698; fY. Yang, Q. Zhao, W. Feng, F. Li, *Chem. Rev.* **2013**, *113*, 192-270; gL. Yuan, W. Lin, K. Zheng, L. He, W. Huang, *Chem. Soc. Rev.* **2013**, *42*, 622-661.

[3] aX. Jiao, Y. Li, J. Niu, X. Xie, X. Wang, B. Tang, *Anal Chem* **2017**; bX. Bai, Y. Huang, M. Lu, D. Yang, *Angew. Chem. Int. Ed. Engl.* **2017**, *56*, 12873-12877; cJ. Zhang, X. Zhen, P. K. Upputuri, M. Pramanik, P. Chen, K. Pu, *Adv. Mater.* **2017**, *29*; dP. Wei, W. Yuan, F. Xue, W. Zhou, R. Li, D. Zhang, T. Yi, *Chem. Sci.* **2018**; eY. H. Chen, T. W. Wei, Z. J. Zhang, W. Zhang, J. Lv, T. T. Chen, B. Chi, F. Wang, X. Q. Chen, *Chinese Chem. Lett.* **2017**, *28*, 1957-1960; fC. C. Chang, F. Wang, J. Qiang, Z. J. Zhang, Y. H. Chen, W. Zhang, Y. Wang, X. Q. Chen, *Sensor Actuat B-Chem* **2017**, *243*, 22-28; gJ. Lv, Y. H. Chen, F. Wang, T. W. Wei, Z. J. Zhang, J. Qiang, X. Q. Chen, *Dyes Pigments* **2018**, *148*, 353-358.

[4] aW. Shu, L. G. Yan, Z. K. Wang, J. Liu, S. Zhang, C. Y. Liu, B. C. Zhu, *Sensor Actuat B-Chem* **2015**, *221*, 1130-1136; bA. C. Sedgwick, H. H. Han, J. E. Gardiner, S. D. Bull, X. P. He, T. D. James, *Chem. Commun.* **2017**, *53*, 12822-12825.

[5] B. Zhu, P. Li, W. Shu, X. Wang, C. Liu, Y. Wang, Z. Wang, Y. Wang, B. Tang, *Anal. Chem.* **2016**, *88*, 12532-12538.

[6] aF. Liu, T. Wu, J. Cao, H. Zhang, M. Hu, S. Sun, F. Song, J. Fan, J. Wang, X. Peng, *Analyst* **2013**, *138*, 775-778; bF. Liu, J. Du, D. Song, M. Xu, G. Sun, *Chem. Commun.* **2016**, *52*, 4636-4639; cH. Xiao, K. Xin, H. Dou, G. Yin, Y. Quan, R. Wang, *Chem. Commun.* **2015**, *51*, 1442-1445; dH. Xiao, J. Li, J. Zhao, G. Yin, Y. Quan, J. Wang, R. Wang, *J. Mater. Chem. B* **2015**, *3*, 1633-1638.

[7] aC. Liu, X. Jiao, S. He, L. Zhao, X. Zeng, *Talanta* **2017**, *174*, 234-242; bL. Liang, C. Liu, X. Jiao, L. Zhao, X. Zeng, *Chem. Commun.* **2016**, *52*, 7982-7985.

[8] H. Wang, X. H. Tian, L. J. Guan, Q. Zhang, S. Y. Zhang, H. P. Zhou, J. Y. Wu, Y. P. Tian, *J. Mater. Chem. B* **2016**, *4*, 2895-2902.

[9] J. Dobkowski, W. Rettig, J. Waluk, *Phys. Chem. Chem. Phys.* **2002**, *4*, 4334-4339.

[10] B. Y. Zhang, Z. X. Jiang, J. Li, Y. N. Zhang, F. Lin, Y. Liu, C. Li, *J. Catal.* **2012**, *287*, 5-12.

[11] M. R. McCall, A. C. Carr, T. M. Forte, B. Frei, *Arterioscl. Throm. Vas.* **2001**, *21*, 1040-1045.

[12] M. Tosa, C. Paizs, C. Majdik, L. Novak, P. Kolonits, F. D. Irimie, L. Poppe, *Tetrahedron-Asymmetr.* **2002**, *13*, 211-221.

[13] aY. Z. Gao, L. F. Zhao, J. Ma, W. H. Xue, H. Zhao, *Eur. J. Pharmacol.* **2016**, *780*, 8-15; bS. R. Liu, S. P. Wu, *Org. Lett.* **2013**, *15*, 878-881; cW. Zhang, W. Liu, P. Li, J. kang, J. Wang, H. Wang, B. Tang, *Chem. Commun.* **2015**, *51*, 10150-10153.

[14] aS. K. Ko, X. Chen, J. Yoon, I. Shin, *Chem Soc Rev* **2011**, *40*, 2120-2130; bA. D. Vliegenthart, C. S. Tucker, J. Del Pozo, J. W. Dear, *Br. J. Clin. Pharmacol.* **2014**, *78*, 1217-1227; cP. Zhang, X. F. Jiang, X. Nie, Y. Huang, F. Zeng, X. Xia, S. Wu, *Biomaterials* **2016**, *80*, 46-56; dY. Huang, P. Zhang, M. Gao, F. Zeng, A. Qin, S. Wu, B. Z. Tang, *Chem. Commun.* **2016**, *52*, 7288-7291.

[15] X. Tian, Q. Zhang, M. Zhang, K. Uvdal, Q. Wang, J. Chen, W. Du, B. Huang, J. Wu, Y. Tian, *Chem. Sci.* **2017**, *8*, 142-149.

[16] aP. Zhang, H. Wang, Y. Hong, M. Yu, R. Zeng, Y. Long, J. Chen, *Biosens Bioelectron* **2018**, *99*, 318-324; bH. Jaeschke, A. Ramachandran, *J. Hepatol.* **2011**, *55*, 227-228.

[17] Z. Mao, H. Jiang, Z. Li, C. Zhong, W. Zhang, Z. Liu, *Chem. Sci.* **2017**, *8*, 4533-4538.

[18] S. Wang, S. Xu, Y. Wang, X. Tian, Y. Zhang, C. Wang, J. Wu, J. Yang, Y. Tian, *Spectrochim. Acta A Mol. Biomol. Spectrosc.* **2017**, *173*, 871-879.

10.1002/chem.201800356

WILEY-VCH

Entry for the Table of Contents

FULL PAPER

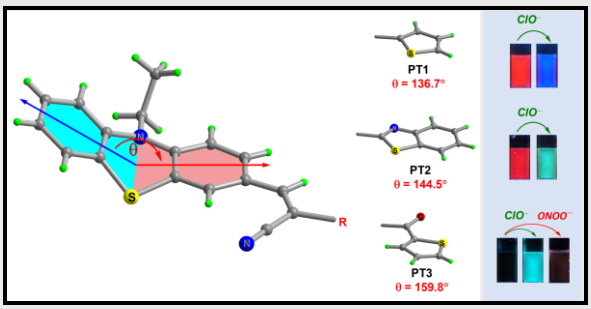

*Shichao Wang, Boyu Zhang, Wenjing Wang, Gang Feng, Daqiang Yuan, * Xuanjun Zhang **

Page No. – Page No.

Elucidating the Structure-Reactivity Correlations of Phenothiazine based Fluorescent Probes toward ClO^-

The sensing mechanisms of a series of phenothiazine based fluorescent probes for ClO^- were studied in detail.